Biochimica et Biophysica Acta 1827 (2013) 1165–1173

Contents lists available at ScienceDirect

Biochimica et Biophysica Acta

journal homepage: www.elsevier.com/locate/bbabio

Highly resolved proton matrix ENDOR of oriented photosystem II membranes in the S_2 state

Hiroki Nagashima, Hiroyuki Mino *

Division of Materials Science (Physics), Graduate School of Science, Nagoya University, Furocho, Chikusa, Nagoya 464-8602, Japan

ARTICLE INFO

Article history:
Received 13 March 2013
Received in revised form 26 May 2013
Accepted 3 June 2013
Available online 14 June 2013

Keywords:
Photosystem II
Oxygen evolving
Mn-cluster
EPR
ENDOR
Photosynthesis

ABSTRACT

Proton matrix ENDOR was performed to investigate the protons close to the manganese cluster in oriented samples of photosystem II (PS II). Eight pairs of ENDOR signals were detected in oriented PS II membranes. At an angle of $\theta = 0°$ between the membrane normal vector $\boldsymbol{n}$ and the external field $\boldsymbol{H_0}$, five pairs of ENDOR signals were exchangeable in D_2O medium and three pairs were not exchangeable in D_2O medium. The hyperfine splitting of 3.60 MHz at $\theta = 0°$ increased to 3.80 MHz at $\theta = 90°$. The non-exchangeable signals with 1.73 MHz hyperfine splitting at $\theta = 0°$, which were assigned to a proton in an amino acid residue, were not detected at $\theta = 90°$ in oriented PS II or in non-oriented PS II. Highly resolved spectra show that only limited numbers of protons were detected by CW-ENDOR spectra, although many protons were located near the $CaMn_4O_5$ cluster. The detected exchangeable protons were proposed to arise from the protons belonging to the water molecules, labeled W1-W4 in the 1.9 Å crystal structure, directly ligated to the $CaMn_4O_5$ cluster, and nearby amino-acid residue.

1. Introduction

In oxygenic photosynthesis, higher plants and cyanobacteria produce molecular oxygen and carbohydrates. Oxygen evolution is catalyzed by a Mn cluster in photosystem II (PS II). Through the absorption of one photon, charge separation occurs in the reaction center of PS II; six chlorophylls, two pheophytin multi-pigment assembly. The electron is transferred to the acceptor quinones, Q_A and Q_B. $P680^+$, the primary oxidant, abstracts an electron from the Mn cluster through tyrosine residue Y_Z. The Mn cluster has five different redox states, labeled S_n ($n = 0$–4). The redox state advances to a higher state (S_n to S_{n+1}) by the absorption of one photon. In the dark, the S_1 state is most stable. During each S state transition, except S_1 to S_2, one or two protons are released. The S_4 state is yet unobserved as intermediate state. Molecular oxygen is evolved during the transition from the S_3 state to the S_0 state [1–3].

Several groups have performed studies to reveal the structure of PS II by X-ray crystal structure analysis [4–6]. Recently, Umena et al. have obtained an X-ray crystal structure of PSII with 1.9 Å resolution and have revealed the atoms that compose the Mn cluster and the coordinated amino acids [7]. The Mn cluster consists of four Mn, five O, and one Ca and is denoted as Mn_4CaO_5. The Mn_4CaO_5 cluster is arranged in a distorted chair form with 3 Mn atoms (Mn1–Mn3) and 1 Ca atom connected by 4 oxygen atoms to form a distorted cubic structure, and the 4th Mn, labeled Mn4, and 5th oxygen (O4) are connected outside of the cubane. It was revealed that two water molecules, labeled W1 and W2, are ligated to the Mn ion (Mn4), and other two water molecules, labeled W3 and W4, are ligated to the Ca ion. The amino acid residues ligated to the Mn ions are D1-H332, D1-D342 and D1-E189 for Mn1, D1-D342, D1-A344 and CP43-E354 for Mn2, D1-E333 and CP43-E354 for Mn3 and D1-D170 and D1-E333 for Mn4. Although the proton network around the Mn cluster was proposed, protons were not detected in the X-ray crystal structure.

Despite the clarification of the fine crystal structure, the mechanism of O_2 evolution is still unclear. Mass spectrometric measurements employing rapid (ms) $H_2^{16}O/H_2^{18}O$ exchange demonstrate that one substrate water molecule is bound to the OEC throughout the Kok cycle, and the water molecule exchanges with an S_n state-dependent half-life that is on the order of seconds. Substrate water that exchanged more quickly was detected in the S_2 and S_3 states [8–10]. Other techniques applied to study water or proton binding include FTIR [11] and NMR [12–14].

EPR is a powerful method to investigate electronic structure. EPR signals were detected for the S_0–S_3 states of the Mn cluster. The S_2 multiline, which arises from four Mn ions of the OEC coupling together creating a ground electronic state with one unpaired electron [15] and has 19–21 peaks at a $g = 2$ center with 60 mT, is the most well-characterized EPR signal among these signals. ^{55}Mn pulsed ENDOR studies have revealed that the Mn cluster arises from a tetramer

Abbreviations: CW, continuous wave; ENDOR, electron nuclear double resonance; EPR, electron paramagnetic resonance; FM, frequency modulation; MES, 2-morpholinoethanesulfonic acid; OEC, oxygen-evolving complex; PS II, photosystem II; RF, radio frequency; Y_D, Tyr161 for higher plants (Tyr160 for cyanobacteria) of the D2 subunit in PS II; Y_Z, Tyr161 of the D1 subunit in PS II

* Corresponding author. Tel./fax: +81 52 789 2882.
E-mail address: mino@bio.phys.nagoya-u.ac.jp (H. Mino).

0005-2728/$ – see front matter © 2013 Elsevier B.V. All rights reserved.
http://dx.doi.org/10.1016/j.bbabio.2013.06.001

and resolved 4 sets of hyperfine interactions of the Mn atoms [16–18]. ESEEM studies have detected the interaction of nitrogen and protons with the Mn cluster [19]. Pulsed EDNMR study primarily showed that the terminal ligands of the Mn4 and at least one μ-oxo bridge exchanges rapidly (seconds timescale) with bulk solvent [20]. ESEEM (HYSCORE) studies have detected the 2–5 sets of proton signals surrounded in the Mn cluster [21–23].

Proton matrix ENDOR is a powerful method to detect the proton signals that surround the Mn cluster. CW-ENDOR strongly depends on the measurement conditions and the nuclear and electron relaxation processes (T_{1n}, T_{1e}, T_{x1} and T_{x2}) [24]. In contrast, pulsed ENDOR, which can be measured under the conditions used to detect spin echoes, does not depend on the relaxation processes. Although the spectral resolution in pulsed ENDOR is relatively low, signals with broader lineshapes are easier to detect. Small hyperfine couplings, such as matrix lines, that are produced by the effects of "distant protons" have low intensity in pulsed ENDOR [25,26]. Changes of peak intensities in pulsed ENDOR are not necessarily only caused by deuterium exchange of the observed protons. CW-ENDOR is free from the so-called blind spot problem in ESEEM and HYSCORE, which make it difficult to interpret the spectra. The CW, pulsed ENDOR and ESEEM techniques give complementary information.

Several CW-ENDOR studies have been performed [27,28]. Kawamori et al. reported that there were six pairs of CW-ENDOR peaks in the S_2 multiline signal [28]. Some of these signals, 2.0 and 4.0 MHz hyperfine separations, were exchangeable in D_2O solution [28]. The ENDOR signals with 4.0 MHz hyperfine splitting have been assigned to the closest proton, which is a distance of 2.7 Å from the Mn cluster, based on the point-dipole approximation. These signals were also detected in a recent pulsed ENDOR study [20]. Yamada et al. reported the multiline CW-ENDOR signals of the S_0 state [29]. The ENDOR spectrum of the S_0 state is very similar to that of the S_2 state, except for the slightly different peak separations [29,30]. This similarity suggests that the spin distributions of the Mn ions are similar in the S_0 and S_2 states for the detected protons. The protons with 4.0 MHz hyperfine splitting show different D_2O exchange rates in the S_0 and S_1 states. The proton exchange rate was fast in the S_0 state, however, it became very slow (longer than 3 h) in the S_1 state. It is important to assign the ENDOR signals arising from protons close to the Mn cluster because characterization of the protons surrounding the Mn cluster is a key to elucidating the mechanism of O_2 evolution. In this study, we performed proton matrix ENDOR by using oriented membranes to assign the ENDOR signals to the protons that, based on the X-ray crystal structure, are close to the Mn cluster.

2. Materials and methods

2.1. Sample preparation

Oxygen-evolving PS II membranes were prepared from market spinach according to the method described previously [31,32]. The obtained PS II membranes were suspended in a medium containing 400 mM sucrose, 20 mM NaCl and 20 mM Mes/NaOH buffer (pH 6.5) and were stored in liquid N_2. The PS II membranes were washed before use with the same medium containing 0.5 mM EDTA·2Na.

For the D_2O exchange treatments, the PS II membranes were washed three times with D_2O buffer containing the same species as the H_2O medium and were incubated for 24 h at 6 °C.

To orient the membranes, the spinach PS II was dried on plastic sheets under humid nitrogen gas flow for 15 h at 4 °C. The sheets were cut into 2.5 × 25 mm^2 pieces, were put into an EPR tube and were frozen immediately. The bottom of the EPR tube was covered with glycerol, which was used to conduct heat during the measurements. To ensure enrichment of the S_1 state, the PS II membranes were dark-adapted for 2–3 h after preillumination. The S_2 state was formed by white light illumination (500 W tungsten lamp) for 5 min at 200 K. All treatments were performed under dim green light at 4 °C.

2.2. EPR measurements

The EPR measurements were performed using a Bruker ESP 300E ESR spectrometer with a gas flow temperature control system (CF935, Oxford Instruments, Oxford, GB). For the ENDOR measurements, the effective linewidth of the FM modulation was measured with a spectral analyzer (R3361C, Advantest, Japan). A 300 mW radio wave from an RF power amplifier (A-300, ENI) was fed to 12 lines of ENDOR coils in the TE_{011} cavity and were terminated with a 50 Ω dummy load [29], which gives good quality for weak couplings at frozen low temperature.

2.3. ENDOR simulations

The ENDOR separation of one unpaired electron and one proton can be described by the hyperfine interaction A between the electron spin and the proton nuclear spin:

$$\nu_{\mathrm{ENDOR}} = |\nu_0 \pm A/2| \tag{1}$$

with

$$A = A_{\mathrm{iso}} + A_{\mathrm{dip}} = A_{\mathrm{iso}} + g\beta g_n\beta_n \frac{\left(1-3cos^2\Theta\right)}{r^3} \tag{2}$$

where A_{iso} is an isotropic Fermi constant that is proportional to the electron spin density that corresponds to the nucleus, A_{dip} is an anisotropic hyperfine interaction determined by space dipole interaction, υ_0 is the Zeeman frequency of the free proton, g and g_n are the g-values of the electron and proton, respectively, and β and β_n are the Bohr magnetons of the electron and proton, respectively. r is the vector between the proton nuclear spin and the electron spin, and Θ is the angle between r and the external static magnetic field $\boldsymbol{H_0}$.

Actually, the electron spin is distributed over the whole Mn cluster. The ENDOR spectrum is found by integrating the hyperfine interactions between the delocalized electron spin and the nuclei. Assuming that electron spins are delocalized on only four Mn ions, the dipole interaction is expressed as:

$$A = A_{\mathrm{iso}} + \sum_i \rho_i A_{\mathrm{dip},i} \tag{3}$$

$$A_{\mathrm{dip},i} = g\beta g_n\beta_n(l,m,n)\begin{bmatrix} \left(r_i^2-3x_i^2\right)/r_i^5 & -3x_iy_i/r_i^5 & -3x_iz_i/r_i^5 \\ -3x_iy_i/r_i^5 & \left(r_i^2-3y_i^2\right)/r_i^5 & -3y_iz_i/r_i^5 \\ -3x_iz_i/r_i^5 & -3y_iz_i/r_i^5 & \left(r_i^2-3z_i^2\right)/r_i^5 \end{bmatrix}\begin{pmatrix} l \\ m \\ n \end{pmatrix}$$

$$= g\beta g_n\beta_n \frac{\left(1-3cos^2\Theta_i\right)}{{r_i}^3} \tag{4}$$

where ρ_i is the spin projection at the i-th (i = 1–4) Mn atom of the Mn cluster, $\mathbf{r}_i$ (x_i, y_i, z_i) is the distance vector between the i-th Mn atom and the proton, and Θ_i is the angle between $\mathbf{r}_i$ and the external magnetic field, and (l, m, n) is the direction cosine of $\boldsymbol{H_0}$ vector. Θ_i is expressed as

$$\cos\Theta_i = \frac{\boldsymbol{H_0}\cdot\boldsymbol{r_i}}{|\boldsymbol{H_0}||\boldsymbol{r_i}|} \tag{5}$$

When $\boldsymbol{H_0}$ is expressed as ($H_0\sin\zeta\cos\eta$, $H_0\sin\zeta\sin\eta$, $H_0\cos\zeta$), the ENDOR signal amplitude $I'(\nu)$ is a function of $\nu(\zeta, \eta)$. ENDOR spectrum $I(\nu)$ is given by integrating $I'(\nu)$ over all directions of $\boldsymbol{H_0}$. In

oriented PS II samples, the ENDOR intensities $I(\nu)$ are given by:

$$I(\nu) = \iint I'(\nu(\zeta,\eta))G(\theta-\zeta)sin\zeta d\zeta d\eta \quad (6)$$

with

$$G(\theta-\zeta) = \frac{1}{\sqrt{2\pi}\Delta} exp\left[-\frac{(\theta-\zeta)^2}{2\Delta^2}\right] \quad (7)$$

where θ is the angle between the membrane normal vector $\boldsymbol{n}$ and the external magnetic field for the observation, $G(\theta-\zeta)$ is the mosaic spread function, which is assumed to be Gaussian, and Δ is the distribution angle of the mosaic spread. The z-axis was set parallel to the membrane normal vector $\boldsymbol{n}$, as was the pseudo C_2 symmetric axis of PS II.

The ENDOR pattern depends on the position of the proton relative to that of the electron. Fig. 1 shows the ENDOR patterns for the dipole interaction between one proton and one electron at 4 Å, where the proton is directed from the electron toward (a) the membrane normal $\boldsymbol{n}$ ($\theta_0 = 0°$) and (b) the membrane plane ($\theta_0 = 90°$) and is detected at an angle between the membrane normal $\boldsymbol{n}$ and the external magnetic field $\boldsymbol{H_0}$ of $\theta = 0°$ and 90°, respectively. Trace (c) shows the powder pattern. In the case of (a) $\theta_0 = 0°$, only the $A_{//}$ and $A_\perp$ components are detected at $\theta = 0°$ and 90°, respectively. In the case of (b) $\theta_0 = 90°$, the $A_\perp$ components are detected at $\theta = 0°$, and both the $A_{//}$ and $A_\perp$ components are detected at $\theta = 90°$. The spectral pattern changes at $\theta_0 = 54.7°$, the so-called magic angle, at which the dipole interaction is lost. This is the general ENDOR pattern for the oriented membranes. In the presence of the electron spin density distribution, ENDOR spectra show rhombic pattern.

In ENDOR simulations, the spin density distribution ρ on each Mn atom should be considered. The spin density distribution is expressed by the vector projection of the local spin $\boldsymbol{S_i}$ to the total spin $\boldsymbol{S_T}$ by the following equation:

$$\rho_i = \frac{\langle S_i \bullet S_T \rangle}{S_T(S_T+1)} \quad (8)$$

The spin projections were experimentally estimated as the ratio of the hyperfine splitting of each Mn in the $CaMn_4O_5$ cluster to that of monomeric Mn. Although some differences have been reported in different models, the absolute values of the spin projections on the Mn1, as Mn(III), and on the Mn2-4, as Mn(IV), atoms may be estimated to be approximately 2 and 1, respectively. ESEEM results suggested that Mn1, labeled in the 1.9 Å resolution crystal structure, is Mn(III) with a spin projection of 2 [19]. Through DFT calculations, Ames et al. have reported the isotropic components of the spin projections to be 1.65, −0.97, −0.94 and 1.27 for Mn1-4, respectively [33]. Based on a PELDOR study, Asada et al. have assigned the isotropic components of the spin projections to be 1.97, −1.20, 1.19 and −0.96 for Mn1-4, respectively [34].

3. Results

3.1. EPR signals in oriented PS II membranes

Fig. 2 shows the EPR signals in the oriented PS II membranes. Panel A shows the angular dependence of the $Y_D^\bullet$ signals in the S_1 state. These signals are observed at angles of (a) $\theta = 0°$, (b) 30°, (c) 60° and (d) 90° between the external field vector $\boldsymbol{H_0}$ and the

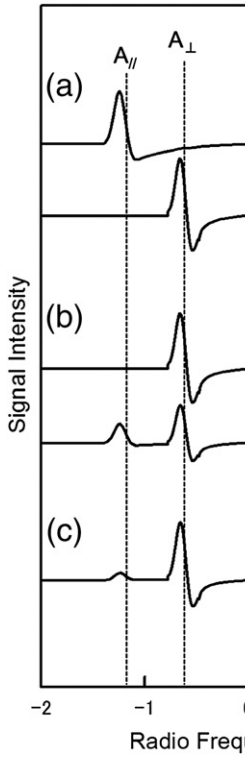

Fig. 1. Simulated ENDOR spectra for a single proton located 4 Å from an electron using (a, b) oriented samples and (c) non-oriented samples. Protons are located in the (a) membrane normal direction and (b) membrane plane.

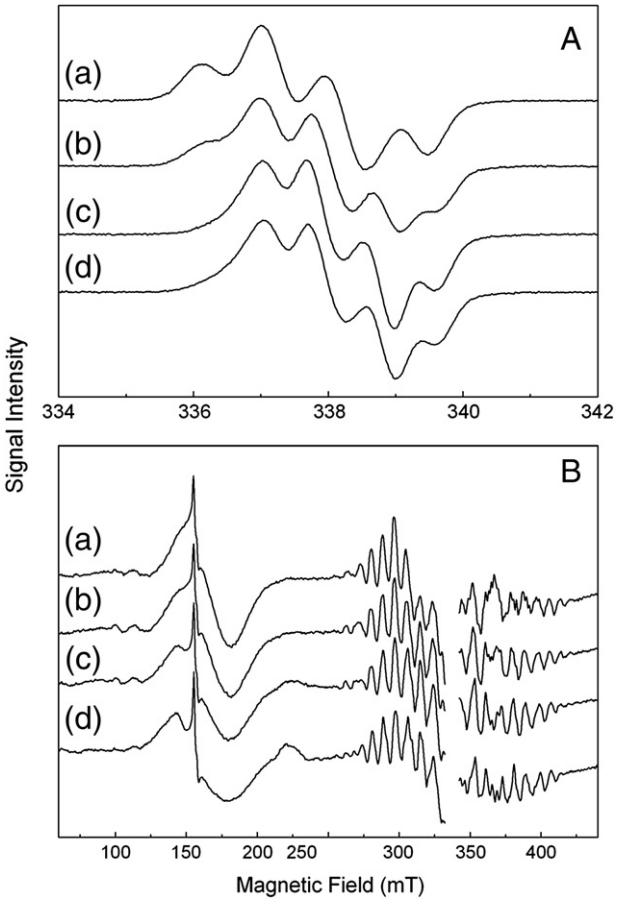

Fig. 2. CW-EPR spectra of oriented PS II membranes observed at an angle θ between the membrane normal **n** and external magnetic field $\boldsymbol{H_0}$ of (a) 0°, (b) 30°, (c) 60° and (d) 90°, respectively. The $Y_D^\bullet$ signals (Panel A) were observed in the S_1 state. Panel B was observed in the S_2 state. Experimental conditions: microwave frequency, 9.44 GHz; microwave power, 0.2 mW; modulation frequency, 100 kHz; modulation amplitude, (A) 0.4 mT and (B) 0.8 mT; temperature, (A) 165 K and (B) 5.5 K.

membrane normal vector $\boldsymbol{n}$. The signals (panel B) centered at $g = 2$ in the range of 260–430 mT arise from the S_2 state of the Mn cluster and are called the S_2 multiline. To suppress the FeQ_A^- signal, the sample was incubated at 77 K in the dark after illumination for 1 week [35]. The angular dependence of the multiline signal in panel B is almost the same as observed in previous studies [36]. The other S_2 state EPR signals are observed around $g = 4$ with a width of 50 mT and show angular dependence [37]. The signal observed at 220–240 mT arises from the g_z components of Cyt. b_{559}, which are used to monitor the mosaic spread angles of the membrane orientation [36]. The angular dependence of the signal intensities were fitted by the Gaussian function defined in Eq. (5); the mosaic spread angle was estimated to be 17° [34]. The ordering condition is higher than in previous reports [36].

3.2. ENDOR spectra of the S_2 multiline signal in oriented PS II membranes

Fig. 3 shows the CW-ENDOR spectra of the S_2 multiline signal in (a, b) oriented PS II membranes and (c) non-oriented PS II membranes. Traces (a) and (b) are observed at angles of (a) $\theta = 0°$ and (b) 90° between the external magnetic field vector $\boldsymbol{H_0}$ and the membrane normal vector $\boldsymbol{n}$, respectively. Trace (c) is consistent with previous reports, in which 6 pairs of ENDOR signals, labeled aa'–ff', are observed [28,29]. The ee' peaks, which were broad and were previously supposed to be a single pair of signals, are composed of two overlapping signals; the inner and outer peaks have hyperfine constants of 2.0 and 3.0 MHz, labeled e_1e_1' and e_2e_2', respectively. Previous reports showed that the ee' and ff' signals were exchangeable in D_2O [28,29]. The spectrum of the oriented membranes observed at $\theta = 90°$ (trace b) is similar to that of the non-oriented membrane (trace c) because the angle Θ, which is between the dipole vector $\boldsymbol{R}$ and the external magnetic field vector $\boldsymbol{H_0}$, involves various geometries in the membrane plane observed at $\theta = 90°$. The spectrum in the oriented membranes observed at $\theta = 0°$ (trace a) is highly resolved because the angle Θ is equal to θ_0 and is uniquely determined, in the extent of the orientation distribution, when observed at $\theta = 0°$. In addition, the new peaks, separated by 1.73 MHz and labeled gg', were detected at $\theta = 0°$ (trace a) and were not detected in the oriented membrane at $\theta = 90°$ (trace b) or in the non-oriented sample (trace c). Through comparison with the typical ENDOR pattern in the oriented membrane shown in Fig. 1, the gg' signals can be easily

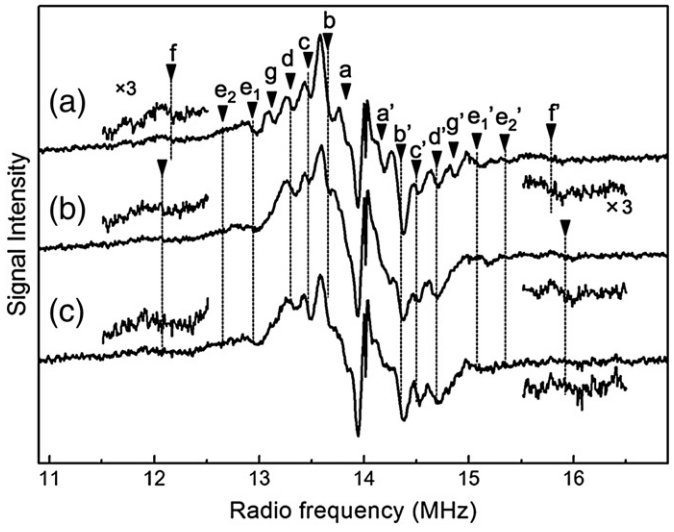

Fig. 3. ENDOR spectra of the S_2 multiline signal in oriented PS II membranes at an angle of (a) 0° and (b) 90° and (c) in the non-oriented PS II membranes. Experimental conditions: microwave frequency, 9.44 GHz; microwave power, 0.8 mW; FM depth, 199.95 kHz; temperature, 5.5 K; magnetic field, 327.7 mT.

assigned to the $A_{//}$ hyperfine components, which are approximately directed to the membrane normal vector $\boldsymbol{n}$ from the electron on Mn cluster. Although the resolution in the spectrum at $\theta = 0°$ (trace a) is very high, the positions of the aa'-ee' peaks do not change significantly. However, the ff' peaks show angular dependence; the separation is 3.6 MHz at $\theta = 0°$ (trace a) and 3.8 MHz at $\theta = 90°$ (trace b). These hyperfine splittings are listed in Table 1.

Fig. 4 shows the CW-ENDOR spectra observed at $\theta = 0°$ of the oriented PS II in (a) H_2O buffer and (b) D_2O buffer. The bb', dd', e_1e_1', e_2e_2' and ff' peaks disappeared in the D_2O buffer, and the peaks were ascribed to the exchangeable protons. However, the cc' and gg' peaks did not disappear in the D_2O medium. Therefore, it was concluded that the gg' peaks arose from the protons of the amino acids close to the Mn cluster. Fig. 5 shows the ENDOR spectra observed at $\theta = 90°$ of the oriented PS II in (a) H_2O buffer and (b) D_2O buffer. As shown in Fig. 4, the bb', e_1e_1', e_2e_2' and ff' peaks disappeared in the D_2O buffer. However, the dd' peaks were not exchangeable. Therefore, it was concluded that the dd' peaks in the non-oriented membranes are composed of overlapping exchangeable and non-exchangeable protons. The dd' peaks observed at $\theta = 0°$ (Fig. 4a) are ascribed to the $A_{//}$ hyperfine components of an exchangeable proton, which is directed to the membrane normal $\boldsymbol{n}$ from the electron on the Mn cluster. The dd' peaks observed at $\theta = 0°$ (Fig. 4a) can be combined with the bb' peaks at $\theta = 90°$ (Fig. 5a) as the $A_{\perp}$ hyperfine components. The dd' peaks observed at $\theta = 90°$ (Fig. 5b) are ascribed to the $A_{//}$ components of a non-exchangeable proton, which is directed toward the membrane plane from the electron on the Mn cluster. In this case, the $A_{\perp}$ components can be ascribed to the bb' peaks at $\theta = 90°$ (Fig. 5b) and $\theta = 0°$ (Fig. 4b).

4. Discussion

4.1. CW-ENDOR detection of protons close to the Mn cluster

Recent structural analysis of PS II with a resolution of 1.9 Å revealed not only the locations of the individual metal ions but also the presence of the oxo-bridges connecting the metal ions and gave rise to a chemical formula of $CaMn_4O_5$ for the OEC. However, the X-ray structure does not show the positions of protons. ENDOR is able to detect protons within 6–7 Å of the $CaMn_4O_5$ cluster. Fig. 6 shows the $CaMn_4O_5$ cluster and the nearby oxygen atoms, which attach exchangeable water molecules. Because the X-ray crystal structure does not give the location of protons, we assumed that the length of the covalent O – H bond is 1.0 Å and, based on the crystal structure, that the water molecules have a hydrogen bond to another oxygen atom. Twelve water molecules within 5 Å of the Mn cluster, labeled W1, W2, W3, W4, W428, W446, W538, W539, W542, W543, W548 and W923 in PDB3ARC, were candidates for matrix ENDOR. Two water molecules, labeled W1 and W2, are directly ligated to Mn4. W3 and W4 are directly ligated to Ca. W1 has hydrogen bonds to Asp61 and Ser169. W2 connects to W446 and W428 by hydrogen bonds. Other water molecules do not directly connect to the $CaMn_4O_5$ cluster. Although many proton signals could overlap in the spectra, the ENDOR region within 2 MHz is fairly well-resolved in oriented PS II membranes observed at $\theta = 0°$. The observed linewidth Δ_{obs} was approximately 100 kHz for peaks aa'–dd' and gg', 130 kHz for peaks e_1e_1' and e_2e_2', and 350 kHz for peaks ff'. The linewidth Δ_{obs} can be estimated from the equation $\Delta^2_{obs} = \Delta^2_{int} + \Delta^2_{inst}$, where Δ_{int} is the intrinsic linewidth and Δ_{int} is the instrumental linewidth Δ_{inst}. The linewidth Δ_{inst} was 50 kHz, measured with the spectral analyzer. Therefore, the intrinsic linewidth Δ_{int} was calculated to be Δ_{int} ~85 kHz for peaks aa'–gg', 120 kHz for e_1e_1'/e_2e_2' and 345 kHz for ff', respectively. The intrinsic linewidths Δ_{int} are the sum of the intrinsic linewidths caused by the relaxation process $1/T_{1n}$ and the distributions of the dipole interactions. If we neglect the linewidth of $1/T_{1n}$, then based

Table 1
Peak separations of the ENDOR measurement in the oriented and non-oriented PS II membranes.

Peaks	aa'	bb'	cc'	dd'	gg'	e1e1'	e2e2'	ff'
Peak separation at $\theta = 0°$ (in MHz)	0.32	0.70	1.06	1.36	1.73	2.13	2.81	3.60
Exchange	–	○/×	×	○	×	○	○	○
Candidates	Distant	W4($A_\perp$)/His332($A_\perp$)	–	W4($A_{//}$)	Asp170($A_{//}$)	W1($A_\perp$)	W1($A_\perp$) W3($A_{//}$)	W2($A_\perp$)
Peak separation at $\theta = 90°$ (in MHz)	0.32	0.70 0.61 (in D_2O buffer)	1.06	1.36	n.d.	2.23	2.85	3.80
Exchange	–	○/×	×	×	–	○	○	○
Candidates	W3($A_\perp$) Distant	W4($A_\perp$)/His332($A_\perp$)	Asp170($A_\perp$)	His332($A_{//}$)	–	W1($A_\perp$) W3($A_\perp$)	W1($A_\perp$)	W2($A_\perp$)
Non-oriented (in MHz)	0.32	0.70	1.06	1.36	n.d.	2.14	2.90	4.00
Exchange	–	○/×	×	○/×	–	○	○	○
Candidates	W3($A_\perp$) Distant	W4($A_\perp$)/His332($A_\perp$)	Asp170($A_\perp$)	W4($A_{//}$)/His332($A_{//}$)	–	W1($A_\perp$) W3($A_\perp$)	W1($A_\perp$) W3($A_{//}$)	W2($A_\perp$)
Britt et al. [39][a]				1.24		1.95		3.97
Rapatskiy et al. [20][b]						2		
Fiege et al. [27]		0.6	1.1			2.3		4.2
Åhrling et al. [21][a]				1.3			2.5	4.2
Martinez et al. [22][c]						2.3		3.7
Milikisiyants et al. [23][d] (in MHz)		0.7 (H_{III})	1.0 ($_{HV}$)			2.1 (H_{IV})	2.6 (H_I)	4.0 (H_{II})

[a] The values were derived from ^2H hyperfine ($A_\perp$).
[b] The value ($A_\perp$) was derived from the $A_{//}$ component.
[c] The values were derived from ($A_\perp$ or A_y components).
[d] The numbering of the protons are based on ref. [23].

on Eq. (3), we can estimate the approximate distribution of the dipole interaction by:

$$\left|\frac{\Delta A}{A}\right| = 3\left|\frac{\Delta r}{r}\right| \quad (9)$$

where Δr and ΔA are the distance distribution and the line broadening, respectively. A distribution of 0.08 Å at a distance of 4 Å causes a line broadening of Δ_{int} approximately 74 kHz. The estimate shows that the observed CW-ENDOR signals arise from protons that are tightly fixed relative to the $CaMn_4O_5$ cluster. Assuming a distance distribution of 0.2 Å, the linewidth becomes 185 kHz, which would be difficult to detect in CW-ENDOR within 3 MHz separation because of other overlapping signals. For the ff' peaks, a distance of 2.7 Å was estimated by the point-dipole approximation, and a distribution of 0.08 Å gives a line broadening of 360 kHz, which is in good agreement with the experiment. The estimate indicates that not all the protons near the $CaMn_4O_5$ cluster can be detected in the CW-ENDOR spectra; this effect is caused by the line-broadening of the distance distribution. In contrast, pulsed ENDOR studies have shown unresolved proton signals in the matrix region [20,30], and all the proton signals in this region were D_2O exchangeable [30]; these results are inconsistent with the CW-ENDOR results. Therefore, it may be concluded that pulsed ENDOR has detected more protons than CW-ENDOR and that the signals for non-exchangeable protons are too small to detect with pulsed ENDOR.

4.2. Exchangeable protons bb', e_1e_1', e_2e_2' and ff'

In addition to W1–W4, which are directly ligated to $CaMn_4O_5$ cluster, eight water molecules, labeled W428, W446, W538, W539, W542, W543, W548 and W923, can be detected by ENDOR in the matrix region. These proton signals overlap within 3 MHz splitting and might be detected in pulsed ENDOR as background signals. Therefore, we assumed that the detected proton signals in CW-ENDOR are only caused by the protons of W1–W4 because these water molecules are directly

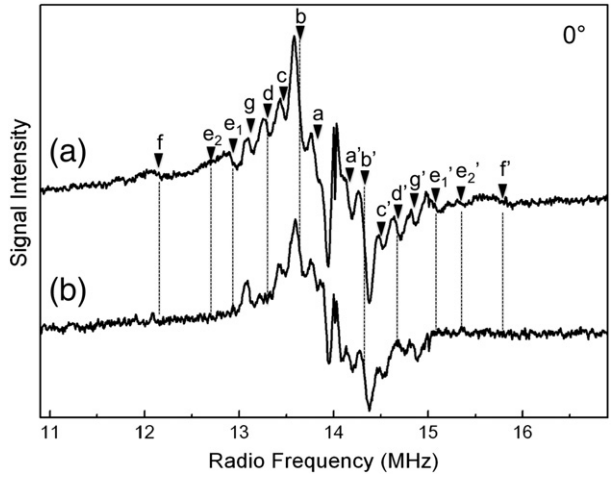

Fig. 4. ENDOR spectra of the S_2 multiline signal in (a) H_2O- and (b) D_2O-treated oriented PS II membranes observed at the angle of $\theta = 0°$. Experimental conditions are the same as in Fig. 3.

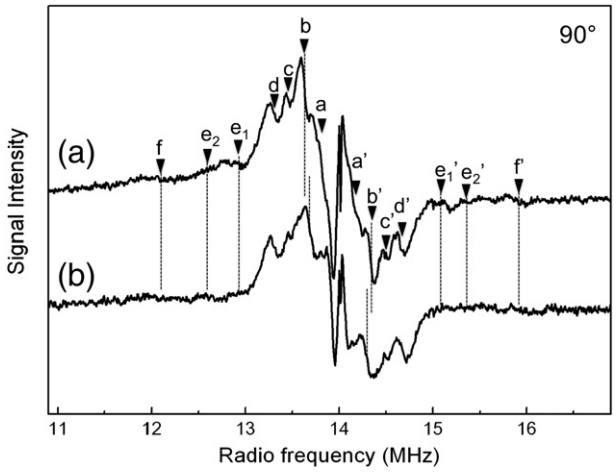

Fig. 5. ENDOR spectra of the S_2 multiline signal in (a) H_2O- and (b) D_2O-treated oriented PS II membranes observed at the angle of $\theta = 90°$. Experimental conditions are the same as in Fig. 3.

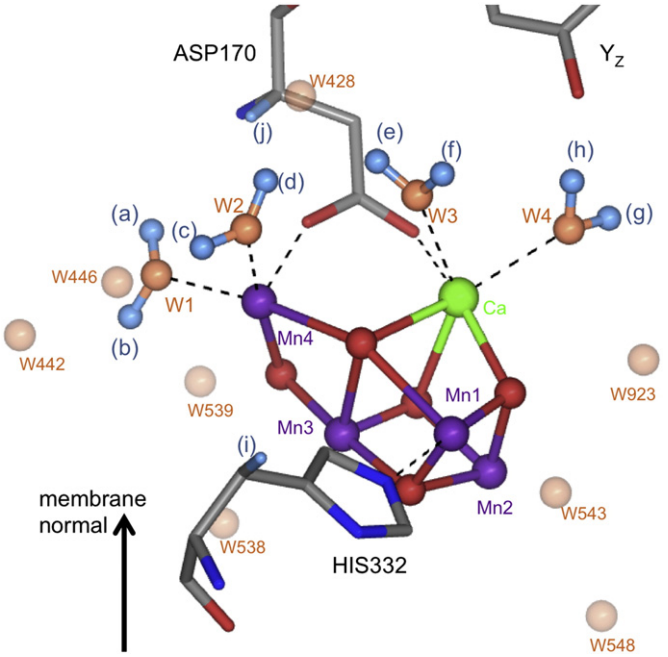

Fig. 6. The structure of the Mn cluster and nearby species determined by X-ray crystal structure analysis (PDB:3ARC). The atom coloring is as follows: Mn, purple; Ca, green; O (water), orange; O (others), red; N, blue; C, gray; H, light blue.

ligated to the Mn cluster and immobilized positions relative to the $CaMn_4O_5$ cluster are expected.

Fig. 7 shows the experimental and simulated ENDOR spectra for (a, b) W1, (c, d) W2, (e, f) W3 and (g, h) W4 in oriented PS II membranes at $\theta = 0°$. The spin projections for Mn ions in ref. [34] were used. The peak separations for the two W1 protons connected to Ser169 and Asp61 were estimated to be (a) 2.6 and (b) 3.4 MHz,

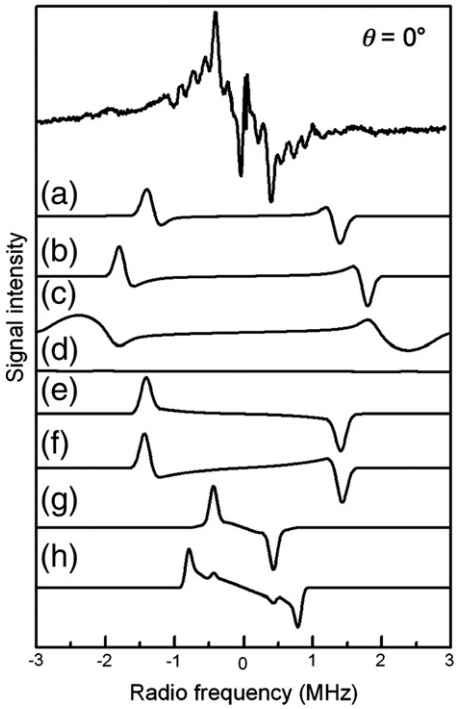

Fig. 7. Comparison between (a) experimental and (b–j) simulated ENDOR spectra in oriented PS II membranes observed at $\theta = 0°$. Trace *a* is the same as trace *a* in Fig. 4. Each proton belongs to (a, b) W1; (c, d); W2; (e, f), W3; (g, h) W4, respectively. The locations of these protons are shown in Fig. 6.

respectively. The peak separation for the W2 proton connected to W446 was estimated to be (c) 4.3 MHz. Another W2 proton connected to W428 was undetectable in this region at $\theta = 0°$ (trace d). The peak separations for the W3 protons, connected to (e) W428 and (f) W542, were 2.7 MHz. The peak separations for the W4 protons, connected to (g) Gln165 and (h) Y_Z, were estimated to be 0.80 and 1.54 MHz, respectively. By comparison with the experimental spectrum, the W1–W4 protons are good candidates for the exchangeable ENDOR peaks, bb', dd', e_1e_1', e_2e_2' and ff'. These protons are candidates for the ff' peaks with 3.6 MHz separation and the e_2e_2' peaks with 3.0 MHz hyperfine splitting. The W4 protons are candidates for the bb' and/or dd' peaks.

Fig. 8 shows the orientational dependence of each CW-ENDOR spectra shown in Fig. 7. The dotted and bold lines show the spectra at $\theta = 0°$ and 90°, respectively. The peak separations of the W1 protons became small at $\theta = 90°$ (a, b). On the other hand, the peak separations of one of the W2 protons became larger at $\theta = 90°$ (c). Therefore, we assigned the ff' peaks to the W2 proton. The peak's positions were qualitatively in agreement with the experimental results. The angular dependence of the W2 proton is in good agreement with the ff' peaks in the experimental ENDOR spectra. The ff' peaks have shifts of 3.6 and 3.8 MHz at $\theta = 0°$ and $\theta = 90°$, whereas the peaks in the simulation (trace c) have shifts of 4.3 and 4.6 MHz at $\theta = 0°$ and $\theta = 90°$. Isotropic hyperfine constants of approximately 0.7 MHz could be included in the fitting process [20,30]. However, the splitting is very sensitive to the proton location and spin projections on the Mn ions, therefore, small differences may not be essential in the present simple model.

There is the other possibility that ff' protons are arising from W543, which is close to the Mn1 and geometrically similar to W2 relative to Mn cluster in the oriented membrane. Although W543 protons are bulk water molecule and slightly far from Mn atoms, the larger spin projection on Mn1 ($\rho \sim 2$) could give them large 4 MHz dipole interaction. It may remain ambiguous. However, the exchange rate of ff' proton is slow (hours) and show S-state dependence [29]. These properties are not suitable for bulky W543.

The separation of the W3 protons is approximately 2.7 MHz at $\theta = 0°$ (e, f), which is assigned to the $A_{//}$ component. One W3 proton, connected to W428, has 0.24 MHz separation at $\theta = 90°$ (trace e). The other W3 proton, connecting with W542, exhibits two pairs of peaks with 0.84 and 2.0 MHz separation at $\theta = 90°$ (trace f). Therefore, we assigned the aa' peaks with 0.32 MHz separation to the W3 proton that is connected to W428, and the e_1e_1' peaks and bb' peaks to the W3 proton that is connected to W542. All experimental peak separations and candidate protons were listed in Table 1.

4.3. Non-exchangeable protons bb', cc', dd' and gg'

There are some non-exchangeable protons labeled aa', bb', cc' and gg', which were observed at $\theta = 0°$, and labeled aa', bb', cc' and dd', which were observed at $\theta = 90°$. In this paper, we do not discuss the angular dependence of the aa' peaks because it is difficult to interpret. The gg' peaks were only observed at $\theta = 0°$. These protons can be ascribed to the protons of an amino acid residue. The narrow linewidth of the gg' peaks may be caused by protons that are tightly immobilized relative to the $CaMn_4O_5$ cluster. However, it is difficult to uniquely specify the protons responsible for these peaks. Tentatively, we assigned the dd' peaks to the C_β proton of His332 and the gg' peaks to the C_α proton of Asp170, which may be relatively immobile. Fig. 9 shows the ENDOR simulations of these protons. Although there are slight differences between the $C_{\beta1}$ and $C_{\beta2}$ protons, only one of the protons was shown.

4.4. Comparison with previous EPR works

Up to date, many EPR works, such as CW-, Pulsed ENDOR and ESEEM (HYSCORE), have been performed to obtain information for

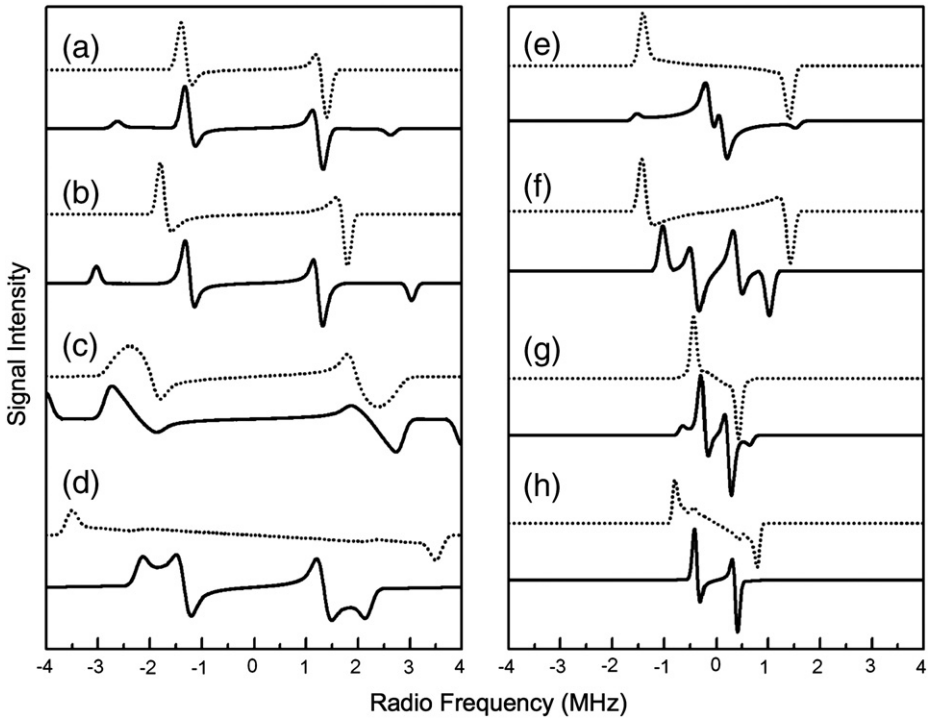

Fig. 8. Angular dependence of the protons belonging to the water molecules ligated to Mn cluster. Each proton belongs to (a, b) W1; (c, d); W2; (e, f), W3; (g, h) W4, respectively. See the text for details.

protons surrounding Mn-cluster [20–23,28–30,38]. These techniques give detail information around Mn-cluster, however, it is difficult to obtain the resolved spectra. By using ESEEM measurements, Åhring et al. have reported 4 sets of hyperfine signals for exchangeable protons surrounded in Mn-cluster, which corresponded to peaks dd', ee' and ff' signals in CW ENDOR [21]. Martinez et al. have reported 2 sets

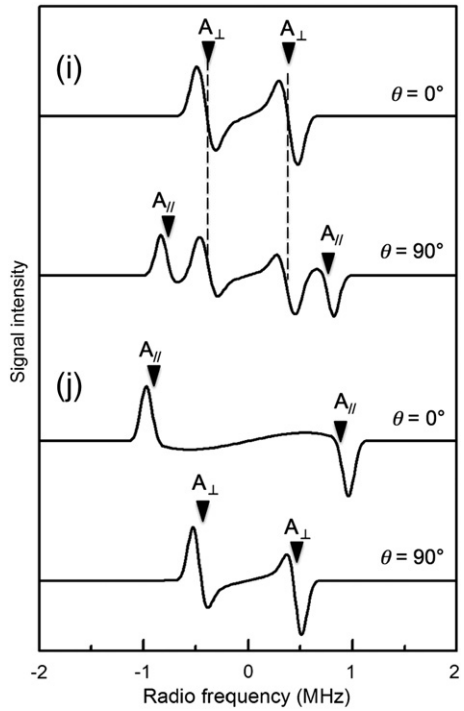

Fig. 9. Angular dependence of the (i) C_β proton of His332 and the (j) C_α proton of ASP170. The locations of these protons are shown in Fig. 7. See the text for details.

of hyperfine signals for protons that surrounded in Mn-cluster, which corresponded to peaks ee' and ff' signals in CW ENDOR [22]. Recently, HYSCORE measurements showed the well-resolved spectra for proton signals [23]. The obtained hyperfine separations are very similar to our CW-ENDOR spectra [28,29], where isolated five proton signals, 2.6, 4, 0.7, 2.1, 1 MHz, labeled $H_{I\text{-}V}$, correspondence to $A_{//}$ peaks, labeled aa'–ff' peaks in CW-ENDOR. Milikisiyants et al. have discussed the assignments of the proton signals with 1.9 Å crystal structure [23]. They have assigned H_I protons to W1(W2), H_{II} protons to D1-His332 or W3,4, H_{III} protons to W1(W2), H_{IV} protons to D1-His337 or Arg357, respectively [23]. As for H_I protons, isotropic hyperfine constants have been used for simulation, where $A_{//} = 10.6$ MHz, $A_\perp = 2.6$ MHz. It is qualitatively consistent with recent pulsed ENDOR results, where the fast exchangeable protons have been detected with hyperfine splittings of $A_{//} = 10$–12 MHz, $A_\perp = 1$–2 MHz [20,30,39]. The signals were assigned to W1(W2) water protons [20,23]. The signals corresponded to the ee' peaks in CW ENDOR, which is consistent with the results that the exchange rates of the ee' protons are fast, which supports that the ee' peaks arise from W1 protons. Although we evaluated only dipole interaction in this paper, it would be possible to include these parameters by slight modification of the proton positions or spin projection on Mn atoms. As for H_{II} protons, D1-His332 protons are non-exchangeable and the orientation dependence for D1-His332 protons does not fit with exchangeable protons, and W3,4 are actually far from Mn ions [23]. We estimated the dipole interaction between Mn ions and W3,4 are within 2 MHz for $A_\perp$ components (e–g in Fig. 8). We assigned the ff' signals to W2 proton. EDNMR spectroscopy has detected three classified fast exchangeable ^{17}O signal, assigned to W1-4 and μ-oxo water [20]. However, the slow exchange rate of the ff' signals shows that the protons are not directly related to water molecule detected by EDNMR signals. As for H_{III}, the peaks were assigned to W1(W2) protons [23]. We observed the overlapping of the two signals on bb' (H_{III}) peaks. These signals are difficult to separate in powder HYSCORE spectrum. Besides, HYSCORE should be checked carefully the artifact arising from

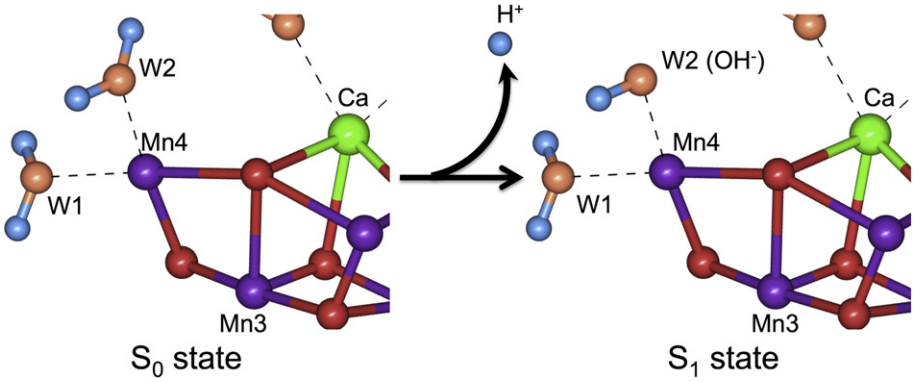

Fig. 10. The model for deprotonation during the transition from the S_0 state to the S_1 state. The atom coloring is the same as in Fig. 7. See the text for details.

blind-spot. We tentatively assigned the peaks to the overlapping of W4 and His332 (bb' and dd'). Further study using different samples slightly modified by biochemical treatments would help precisely assign the ENDOR signals.

4.5. Properties of the ff' protons

The valences of the Mn ions in the $CaMn_4O_5$ cluster are proposed to be 3Mn(III)1Mn(IV) for S_0 state, 2Mn(III)2Mn(IV) for S_1 state and 1Mn(III)3Mn(IV) for S_2 state[1–3]. Yamada et al. have previously reported that the exchange rate of the ff' proton is very slow in S_1 state but is fast in the S_0 state [29]. The oxidation of the Mn attached to the ff' proton has been proposed. In this paper, we assigned the ff' peaks to the W2 proton ligated to Mn4. Therefore, the lowering of the exchange rate might be caused by the deprotonation of W2. Based on the ENDOR simulations, a W2 proton connected to W446 was assigned to the ff' proton, so the other W2 proton connected to W428 could be released. This proposal supports the experimental result that the exchange rate of the W1 protons, which are connected to Mn4, is still fast in S_1 state. Fig. 10 shows the model for the transition from the S_0 to S_1 states. Recent DFT calculations have proposed the OH^- ligand to Mn4 in S_1 state [33,40–42], and deprotonation for the transition from S_0 to S_1 states [41,42]. In Mn model complexes the exchange rate of terminal water/hyrdoxo ligands of MnIII complexes with bulk water is as yet unresolved [43,44]. Hiller and Wydrzynski have shown that the exchange rate of water oxygen ligating to metal M^{n+1} is 10^4 times slower than that to metal M^n [9]. Therefore, the slow exchange rate is preferable to be caused by not only deprotonating, but also oxidation of the ligating Mn atom. Ames et al.'s DFT model has reported that Mn4 is not oxidized in the transition of S_0/S_1 states [33]. It is consistent with the Sigbahn's DFT model and FTIR results, where Mn4 is insensitive to the replacement of Asp170 [45]. It is consistent with Rapatskiy et al.'s assignments, where they assigned fast exchangeable water as W2 based on DFT model. On the other hand, Yamaguchi et al. have recently reported that the Mn4 is oxidized from Mn(III) to Mn(IV) in the transition of S_0/S_1 states[46,47]. This model supports the behavior of the slow exchange rate of the protons nearby Mn4. Besides, as it does not completely exclude the possibility that exchange rate depends on the species or extrinsic proteins, it is worth measuring the same experiments by using cyanobacteria in the future.

This ENDOR study revealed that the exchange rate of ff' protons is slower than that of the substrate water molecules in S_1 state. All other water molecules, labeled W1, W3 and W4, that are ligated to the Mn cluster, have fast exchange rates in the S_0 and S_1 state. The difference of the A_{iso} for W1 and W2 protons is ascribed to the relative locations of the Mn1–Mn3 and the spin projections. W1 and W2 protons are the closest protons to Mn atoms, and therefore magnitudes are very sensitive to the positions of the protons. Although the orientation dependences of these protons were explained based on the crystal structure in S_1 state and spin projections, A_{dip} changes 3–5 MHz for the difference of ± 0.2 Å. For fitting the exact position of the spectral peaks, the information of the protons' location and A_{iso} should be required. Pulsed ENDOR results show that A_{iso} are estimated as 2 MHz for W1 protons [20]. Supposing W2 is deprotonated in S_1 state, A_{iso} for W2 might be expected as the comparable or larger value to that for W1. If A_{iso} value for W2 was fixed, the precise coordination of W2 proton would be also fixed. However, at present such a detail fitting would be not so much informative in the view of the crystal resolution and DFT calculations.

In this paper, we showed that the CW-ENDOR spectra can be explained only by the directly ligated water protons of W1–W4 and by the protons of some amino acids. The ENDOR simulations involve some ambiguity in the spin projections and proton positions used. Rapatskiy et al. have reported the hyperfine parameters of these protons from DFT calculations [20], whereas we used the proton positions obtained without DFT modeling and an αβαβ spin topology model for the four Mn atoms [34]. Although different models are used in the simulation, the hyperfine separations obtained in our calculation are in qualitatively good agreement with Rapatskiy et al.'s report. This agreement is because the Mn2–Mn4 contribution is almost equivalent to the absolute value of the spin projections, i.e. 2:1:1:1 for Mn1–Mn4. However, the different spin topologies and proton positions around the oxygen atom may influence the orientational dependence of the ENDOR spectra.

In summary, highly resolved proton matrix CW-ENDOR signals of the S_2 multiline signal for oriented PS II membranes were detected, based on the X-ray crystal structure, and were assigned to protons. Assuming that these signals arose from the W1–W4 water protons, the ENDOR peaks were assigned to the protons. These results give a clue to the mechanism of water oxidation.

Acknowledgments

This work was supported by a MEXT/JSPS Grant-in-Aid for Exploratory Research No. 22684051 and the Kurata foundation to H. M., and supported by the Program for Leading Graduate Schools “Integrative Graduate Education and Research in Green Natural Sciences”, MEXT, Japan to H.N.

References

[1] J.P. McEvoy, G.W. Brudvig, Water-splitting chemistry of photosystem II, Chem. Rev. 106 (2006) 4455–4483.
[2] J. Messinger, G. Renger, Photosynthetic water-splitting, in: G. Renger (Ed.), Primary Processes of Photosynthesis-Part2: Basic Principles and Apparatus, Royal Society of Chemistry, Cambridge, 2008, pp. 291–349.
[3] N. Nelson, C.F. Yocum, Structure and function of photosystems I and II, Annu. Rev. Plant Biol. 57 (2006) 521–565.

[4] K.N. Ferreira, T.M. Iverson, K. Maghlaoui, J. Barber, S. Iwata, Architecture of the photosynthetic oxygen-evolving center, Science 303 (2004) 1831–1838.
[5] A. Guskov, J. Kern, A. Gabdulkhakov, M. Broser, A. Zouni, W. Saenger, Cyanobacterial photosystem II at 2.9 Å resolution and the role of quinones, lipids, channels and chloride, Nat. Struct Mol. Biol. 16 (2009) 334–342.
[6] B. Loll, J. Kern, W. Saenger, A. Zouni, J. Biesiadka, Towards complete cofactor arrangement in the 3.0 Å resolution structure of photosystem II, Nature 438 (2005) 1040–1044.
[7] Y. Umena, K. Kawakami, J.R. Shen, N. Kamiya, Crystal structure of oxygen-evolving photosystem II at a resolution of 1.9 Å, Nature 473 (2011) 55–62.
[8] J. Messinger, M. Badger, T. Wydrzynski, Detection of one slowly exchanging substrate water molecule in the S_3 state of photosystem II, Proc. Natl. Acad. Sci. U. S. A. 92 (1995) 3209–3213.
[9] W. Hillier, T. Wydrzynski, Oxygen ligand exchange at metal sites — implications for the O_2 evolving mechanism of photosystem II, Biochim. Biophys. Acta 1503 (2001) 197–209.
[10] G. Hendry, T. Wydrzynski, The two substrate-water molecules are already bound to the oxygen-evolving complex in the S_2 state of photosystem II, Biochemistry 41 (2002) 13328–13334.
[11] T. Noguchi, M. Sugiura, Flash-induced FTIR difference spectra of the water oxidizing complex in moderately hydrated photosystem II core films: effect of hydration extent on S-state transitions, Biochemistry 41 (2002) 2322–2330.
[12] A.N. Srinivasan, R.R. Sharp, Flash-induced enhancements in the proton NMR relaxation rate of Photosystem II particles: response to flash trains of 1–5 flashes, Biochim. Biophys. Acta 851 (1986) 369–376.
[13] T.J. Wydrzynski, Early indications for manganese oxidation state changes during photosynthetic oxygen production: a personal account, Photosynth. Res. 80 (2004) 125–135.
[14] T.J. Wydrzynski, S.B. Marks, P.G. Schmidt, Govindjee, H.S. Gutowsky, Nuclear magnetic-relaxation by manganese in aqueous suspensions of chloroplast, Biochemistry 17 (1978) 2155–2162.
[15] G.C. Dismukes, Y. Siderer, Intermediate of a polynuclear manganese center involved in photosynthetic oxidation of water, Proc. Natl. Acad. Sci. U. S. A. 78 (1981) 274–278.
[16] L.V. Kulik, B. Epel, W. Lubitz, J. Messinger, ^{55}Mn pulse ENDOR at 34 GHz of the S_0 and S_2 states of the oxygen-evolving complex in photosystem II, J. Am. Chem. Soc. 127 (2005) 2392–2393.
[17] J.M. Peloquin, K.A. Campbell, D.W. Randall, M.A. Evanchik, V.L. Pecoraro, W.H. Armstrong, R.D. Britt, ^{55}Mn ENDOR of the S_2-state multiline EPR signal of photosystem II: implications on the structure of the tetranuclear Mn cluster, J. Am. Chem. Soc. 122 (2000) 10926–10942.
[18] L.V. Kulik, B. Epel, W. Lubitz, J. Messinger, Electronic structure of the Mn_4O_xCa cluster in the S_0 and S_2 states of the oxygen-evolving complex of photosystem II based on pulse ^{55}Mn-ENDOR and EPR spectroscopy, J. Am. Chem. Soc. 129 (2007) 13421–13435.
[19] T.A. Stich, G.J. Yeagle, R.J. Service, R.J. Debus, R.D. Britt, Ligation of D1-His332 and D1-Asp170 to the manganese cluster of photosystem II from synechocystis assessed by multifrequency pulse EPR spectroscopy, Biochemistry 50 (2011) 7390–7404.
[20] L. Rapatskiy, N. Cox, A. Savitsky, W.M. Ames, J. Sander, M.M. Nowaczyk, M. Rogner, A. Boussac, F. Neese, J. Messinger, W. Lubitz, Detection of the water-binding sites of the oxygen-evolving complex of photosystem II using W-band ^{17}O electron–electron double resonance-detected NMR spectroscopy, J. Am. Chem. Soc. 134 (2012) 16619–16634.
[21] K.A. Åhrling, M.C.W. Evans, J.H.A. Nugent, R.J. Ball, R.J. Pace, ESEEM studies of substrate water and small alcohol binding to the oxygen-evolving complex of photosystem II during functional turnover, Biochemistry 45 (2006) 7069–7082.
[22] J.I. Martinez, I. Yruela, R. Picorel, P.J. Alonso, ^{1}H hyperfine interactions in the Mn-cluster of photosystem II in the S_2 state detected by hyperfine sublevel correlation spectroscopy, J. Phys. Chem. B 114 (2010) 15345–15353.
[23] S. Milikisiyants, R. Chatterjee, C.S. Coates, F.H.M. Koua, J.R. Shen, K.V. Lakshmi, The structure and activation of substrate water molecules in the S_2 state of photosystem II studied by hyperfine sublevel correlation spectroscopy, Energy Environ. Sci. 5 (2012) 7747–7756.
[24] H. Kurreck, B. Kirste, W. Lubitz, Electrin nuclear double resonance, in: A.P. Marchand (Ed.), Methods in Stereochemical Analysis, VCH Publishers, New York, 1988, pp. 7–80.
[25] A.V. Astashkin, A. Kawamori, Matrix line in pulsed electron-nuclear double resonance spectra, J. Magn. Reson. 135 (1998) 406–417.
[26] G. Schweiger, G. Jeschke, Principles of Pulsed Electron Paramagnetic Resonance, Oxford University Press, Inc., 2001
[27] R. Fiege, W. Zweygart, R. Bittl, N. Adir, G. Renger, W. Lubitz, EPR and ENDOR studies of the water oxidizing complex of photosystem II, Photosynth. Res. 48 (1996) 227–237.
[28] A. Kawamori, T. Inui, T. Ono, Y. Inoue, ENDOR study on the position of hydrogens close to the manganese cluster in S_2 state of photosystem II, FEBS Lett. 254 (1989) 219–224.
[29] H. Yamada, H. Mino, S. Itoh, Protons bound to the Mn cluster in photosystem II oxygen evolving complex detected by proton matrix ENDOR, Biochim. Biophys. Acta 1767 (2007) 197–203.
[30] C.P. Aznar, R.D. Britt, Simulations of the ^{1}H electron spin echo-electron nuclear double resonance and ^{2}H electron spin echo envelope modulation spectra of exchangeable hydrogen nuclei coupled to the S_2-state photosystem II manganese cluster, Philos. Trans. R. Soc. Lond. B Biol. Sci. 357 (2002) 1359–1365.
[31] D.A. Berthold, G.T. Babcock, C.F. Yocum, A highly resolved, oxygen-evolving photosystem-ii preparation from spinach thylakoid membranes — electron-paramagnetic-res and electron-transport properties, FEBS Lett. 134 (1981) 231–234.
[32] T. Ono, Y. Inoue, Effects of removal and reconstitution of the extrinsic 33, 24 and 16 proteins on flash oxygen yield in photosystem II particles, Biochim. Biophys. Acta 850 (1986) 380–389.
[33] W. Ames, D.A. Pantazis, V. Krewald, N. Cox, J. Messinger, W. Lubitz, F. Neese, Theoretical evaluation of structural models of the S_2 state in the oxygen evolving complex of photosystem II: protonation states and magnetic interactions, J. Am. Chem. Soc. 133 (2011) 19743–19757.
[34] M. Asada, H. Nagashima, F.H.M. Koua, J.-R. Shen, A. Kawamori, H. Mino, Electronic structure of S_2 state of the oxygen-evolving complex of photosystem II studied by PELDOR, Biochim. Biophys. Acta 1827 (2013) 438–445.
[35] T. Inui, A. Kawamori, G. Kuroda, T. Ono, Y. Inoue, EPR study of charge recombination via D^+ in the S_2 state of oxygen evolving photosystem II, Biochim. Biophys. Acta 973 (1989) 147–152.
[36] K. Hasegawa, M. Kusunoki, Y. Inoue, T.A. Ono, Simulation of S_2 state multiline EPR signal in oriented photosystem II membranes: structural implications for the manganese cluster in an oxygen-evolving complex, Biochemistry 37 (1998) 9457–9465.
[37] A.W. Rutherford, Orientation of EPR signals arising from components in photosystem II membranes, Biochim. Biophys. Acta 807 (1985) 189–201.
[38] X.S. Tang, M. Sivaraja, G.C. Dismukes, Protein and substrate coordination to the manganese cluster in the photosynthetic water oxidizing complex — ^{15}N and ^{1}H ENDOR spectroscopy of the S_2 state multiline signal in the thermophilic cyanobacterium *Synechococcus elongatus*, J. Am. Chem. Soc. 115 (1993) 2382–2389.
[39] R.D. Britt, K.A. Campbell, J.M. Peloquin, M.L. Gilchrist, C.P. Aznar, M.M. Dicus, J. Robblee, J. Messinger, Recent pulsed EPR studies of the photosystem II oxygen-evolving complex: implications as to water oxidation mechanisms, Biochim. Biophys. Acta 1655 (2004) 158–171.
[40] M. Kusunoki, S_1-state Mn_4Ca complex of photosystem II exists in equilibrium between the two most-stable isomeric substates: XRD and EXAFS evidence, J. Photochem. Photobiol. B 104 (2011) 100–110.
[41] H. Isobe, M. Shoji, S. Yamanaka, Y. Umena, K. Kawakami, N. Kamiya, J.R. Shen, K. Yamaguchi, Theoretical illumination of water-inserted structures of the $CaMn_4O_5$ cluster in the S_2 and S_3 states of oxygen-evolving complex of photosystem II: full geometry optimizations by B3LYP hybrid density functional, Dalton Trans. 41 (2012) 13727–13740.
[42] P.E.M. Siegbahn, Water oxidation mechanism in photosystem II, including oxidations, proton release pathways, O–O bond formation and O_2 release, Biochim. Biophys. Acta 1827 (2013) 1003–1019.
[43] R. Tagore, R.H. Crabtree, G.W. Brudvig, Distinct mechanisms of bridging-oxo exchange in Di-μ-O dimanganese complexes with and without water-binding sites: implications for water binding in the O_2-evolving complex of photosystem II, Inorg. Chem. 46 (2007) 2193–2203.
[44] I.L. McConnell, V.M. Grigoryants, C.P. Scholes, W.K. Myers, P.Y. Chen, J.W. Whittaker, G.W. Brudvig, EPR-ENDOR characterization of (^{17}O, ^{1}H, ^{2}H) water in manganese catalase and its relevance to the oxygen-evolving complex of photosystem II, J. Am. Chem. Soc. 134 (2012) 1504–1512.
[45] R.J. Debus, M.A. Strickler, L.M. Walker, W. Hillier, No evidence from FTIR difference spectroscopy that aspartate-170 of the D1 polypeptide ligates a manganese ion that undergoes oxidation during the S_0 to S_1, S_1 to S_2, or S_2 to S_3 transitions in photosystem II, Biochemistry 44 (2005) 1367–1374.
[46] K. Yamaguchi, H. Isobe, S. Yamanaka, T. Saito, K. Kanda, M. Shoji, Y. Umena, K. Kawakami, J.R. Shen, N. Kamiya, M. Okumura, Full geometry optimizations of the mixed-valence $CaMn_4O_4X(H_2O)_4$ (X = OH or O) cluster in OEC of PS II: degree of symmetry breaking of the labile Mn–X–Mn bond revealed by several hybrid DFT calculations, Int. J. Quantum Chem. 113 (2013) 525–541.
[47] K. Yamaguchi, S. Yamanaka, H. Isobe, T. Saito, K. Kanda, Y. Umena, K. Kawakami, J.R. Shen, N. Kamiya, M. Okumura, H. Nakamura, M. Shoji, Y. Yoshioka, The nature of chemical bonds of the $CaMn_4O_5$ cluster in oxygen evolving complex of photosystem II: Jahn-Teller distortion and its suppression by Ca doping in cubane structures, Int. J. Quantum Chem. 113 (2013) 453–473.